

pubs.acs.org/EF Article

Vacuum Pyrolysis of Hybrid Poplar Milled Wood Lignin with Fourier Transform-Ion Cyclotron Resonance Mass Spectrometry Analysis of Feedstock and Products for the Elucidation of Reaction Mechanisms

Evan Terrell and Manuel Garcia-Perez*



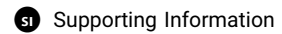
Cite This: Energy Fuels 2020, 34, 14249-14263



ACCESS

III Metrics & More





ABSTRACT: The pyrolysis of lignocellulosic materials is a promising technique to produce fuels and chemicals. It is well known that the most abundant products of lignin pyrolysis are oligomeric molecules, known as pyrolytic lignin (PL). The chemical composition of PL has been extensively studied; however, there is still an important debate whether these oligomers are produced directly from the lignin or from the recombination of monomeric pyrolytic products. Existing theories are unable to describe the effect of vacuum on the distribution of pyrolysis products. Hybrid poplar milled wood lignin (MWL) was initially isolated and thoroughly characterized by Fourier transform-ion cyclotron resonance mass spectrometry (FT-ICR MS). Chemical formulas were assigned to each oligomeric compound detected. The MWL was also subjected to vacuum pyrolysis in a modified pyroprobe at 250, 750, and 1000 mbar (absolute pressure), and the resulting liquid products were analyzed by FT-ICR MS. A new strategy to assign structural representations to the oligomeric PL products is proposed, based on the plausible pyrolysis reaction mechanisms of depolymerization/fragmentation applied to original MWL oligomer formulas. Our results support the hypothesis that PL is formed from the removal of moieties from primary lignin pyrolysis products with between three and five aromatic rings. This depolymerization/fragmentation allows the oligomers to reduce their molecular weights to the point where they can be removed from the reaction zone by direct vaporization. This phenomenon highlights the importance of pressure on removal mechanisms and their impact on the molecular weight of the resulting products from lignin pyrolysis.

1. INTRODUCTION

Lignin is a recalcitrant, heterogeneous polymeric material accounting for roughly 25% of biomass by weight and 40% by energy content.^{1–4} With more carbon and less oxygen than holocellulose, lignin represents the most abundant renewable, naturally occurring source of aromatic molecules.^{2,5} As such, it is the focus of significant research and development aimed at the synthesis of green biofuels and chemicals. $^{1,6-10}$ There are also important distinctions between native and extracted (or technical) lignins, which tend to be more modified with a greater abundance of relatively strong C-C bonds (in comparison with weaker ether bonds). Albishi et al. state (quoted directly) that "there is still much debate on whether any lignin extract adequately represents the native structure," a sentiment that is echoed in an earlier publication from this group on a critique of lignin structural analysis. 11,12 These authors suggest that native lignin is composed of short oligomers connected in a "criss-cross" fashion with holocellulose to form a given wood network. 12,13 Crestini et al., based on results largely from ³¹P NMR analysis, similarly report that milled wood lignin (MWL) is made up of linear oligomers connected primarily by weak ether bonds, 14 although this perspective is challenged in a recent review on lignin biphenyl linkages.15

Canonically, lignin is considered to be formed from the oxidative coupling of three primary monomers: *p*-coumaryl alcohol, coniferyl alcohol, and sinapyl alcohol. ¹⁶ More recently, however, the concept of what makes up lignin, its biosynthesis

and bioengineering, and its form both *in planta* and after extraction has become much more diverse, with new, unique components having been recently identified. $^{12,13,17-19}$ This evolving perspective is largely driven by the advent of much more powerful analytical capabilities. Among the most significant of these analytical techniques is advanced mass spectrometry (MS) analysis. Some recently published work on lignin MS analysis can be found from Bowman et al. (synthesized model oligomers), Qi et al., Kubatova et al., Mikhael et al., and Prothmann et al. $^{13,21-24}$ A particularly robust MS technique for the characterization of complex matrices is Fourier transform-ion cyclotron resonance (FT-ICR) MS, which is capable of assigning molecular formulas (i.e., $C_1H_1O_2$) to detected MS peaks from the m/z value alone. $^{25-28}$ FT-ICR MS has been successfully applied for the characterization and/or description of lignin directly as well as for similar/relevant reactive processes and systems. $^{21,29-36}$

Pyrolysis is a reactive process of great interest to the biomass community in general and lignin researchers in specific. Pyrolysis is the thermochemical deconstruction of an initial feedstock via heating, rapidly, in the case of "fast" or "flash"

Received: August 30, 2020 Revised: September 22, 2020 Published: October 9, 2020





pyrolysis, under an inert atmosphere (most commonly nitrogen).³⁷ During the pyrolysis of whole biomass, roughly half of the lignin-derived products are collected in the form of oligomers. 38,39 There are two main hypotheses as to how these oligomeric products are formed. The first one proposes that oligomers result from the recombination of monomeric lignin pyrolysis products. 40,41 The second hypothesis considers that pyrolytic lignin is produced from the degradation of primary lignin oligomeric products. 42–44 Experimental evidence shows that during lignin pyrolysis, the starting material undergoes swelling, softening, and/or melting at low temperature (<~200 °C), dehydration and side-chain reactions at intermediate temperature ($\sim 200-500$ °C), and aromatic substituent conversion with polycyclic rearrangement at high temperature (>~500 °C). 29,37 From a microkinetic modeling perspective, Yanez et al. report that major reaction families include ether cleavage, demethoxylation, demethanation, decarboxylation, deacylation, dealkylation, aliphatic C-C cleavage, methoxyl isomerization, oxidation, hydrogen addition, and char formation.45 The nonreactive vaporization of low-molecularweight oligomers has also been recently highlighted as an important occurrence during lignin pyrolysis processes. 44,46–48 In this mass-transport-driven phenomenon, oligomeric species with sufficiently low devolatilization temperature (conceptually similar to the normal boiling point) are capable of evaporating/sublimating directly from the reaction front with a limited extent of actual reactions having taken place. 44,49 The effect of pressure on the production of oligomeric lignin products is still poorly understood. Using empirical methods applied to hypothetical molecular structures, it is possible to estimate vaporization curves from the Clausius-Clapeyron equation, thereby suggesting the molecular sizes capable of evaporating at a given pyrolysis temperature.⁴⁷ Importantly, this type of analysis highlights the way in which pressure, which theoretically does not have an effect on chemical reaction kinetics in condensed phases (i.e., solids and liquids), can still greatly affect the properties of collected lignin pyrolysis products. For the pyrolysis of whole wood particles at the millimeter to centimeter scale, pressure has been shown to play a role in the convective mass transport and intraparticle residence time of gas/vapor phase products, whose velocity can be modeled using Darcy's law relationship. Larger internal pressure gradients may also result in the modifications of the biomass particle morphology and porosity during a pyrolysis process.

Studying lignin and its pyrolysis products with FT-ICR MS and linking their structures through proposed fragmentation mechanisms could advance the understanding of pyrolytic lignin and the nature of its formation. The primary advantage of FT-ICR MS in this setting is in its ability to characterize lignin-derived oligomers. Previous work has shown success in the combination of stochastic simulation and FT-ICR MS measurements of MWL.30 This type of approach has also been extended to the characterization of whole biomass pyrolysis oils.⁵⁰ The goal of this work is to utilize FT-ICR MS measurements of both raw MWL and its pyrolysis products to propose the structure representations of pyrolysis-derived oligomers. This structural understanding can then be used as a basis for the modeling and discussion of the primary mechanisms underlying oligomer formation during the pyrolysis processes of diverse feedstocks.

2. METHODOLOGY

2.1. Feedstock and Lignin Preparation. This work draws on the analysis previously carried out in earlier published studies on the characterization of hybrid poplar MWL and its pyrolysis under vacuum conditions. The MWL was prepared in separate batches from a common hybrid poplar biomass sourced from Pasco, WA, donated by the Boise Cascade Corporation. This raw biomass contains 16% acidinsoluble lignin, 3% acid-soluble lignin, 21% mannose, 43% glucose, and <1% arabinose and galactose, with 1% ash and 4% extractives. 52 Lignin was extracted from biomass via solubilization in dioxane/water (~9:1 v/v) from extractive-free milled wood (~0.1 mm particle size), following an adapted Bjorkman method. 53-55 Further details are available elsewhere. 30,51 The images detailing the process of lignin extraction and physical characteristics of the MWL are given in the Supporting Information.

2.2. Lignin Characterization. The MWL was characterized using a range of techniques in previous works, including py-GC/MS, HSQC NMR, and matrix-assisted laser desorption ionization (MALDI)-FT-ICR MS. 30 For FT-ICR MS analysis, MWL was suspended/dissolved in methanol/water (\sim 6:1 v/v) and deposited dropwise onto the instrument sample holder along with a saturated dihdyroxybenzoic acid (DHB) solution. Measurements were then performed on solvent-free lignin (with DHB matrix) using a 9.4 T actively shielded FT-ICR MS instrument (Varian/Ionspec) in the positive ion mode. The collected spectra were internally calibrated using the OMEGA MS instrument software and further compiled and assigned with the Composer software (Sierra Analytics). The relative monomer distribution and β -bond type distribution were determined using py-GC/MS and HSQC NMR, respectively. This information, along with the molecular weight distribution from MALDI-FT-ICR MS, was used to generate a stochastic library of lignin molecules. 56 This computational/hypothetical lignin library was then used as a basis to propose structures for MS-detected oligomer peaks in the analyzed sample.³⁰

2.3. Lignin Pyrolysis. MWL from the same hybrid poplar source material was pyrolyzed at a subatmospheric pressure using a modified pyroprobe reactor setup.⁵¹ The reactor is described in detail in earlier work from Pecha et al., with a schematic shown in Figure 1.57 This reactor can be reliably operated at pressures as low as 5 mbar (absolute pressure); however, high-quality FT-ICR MS product characterization data for runs at this pressure were not available. Experimental pyrolysis studied here occurred on the thin films (\sim 0.1 mm) of MWL (~5 mg) deposited on the internal walls of quartz tubes (2 mm OD) heated by the modified pyroprobe reactor at pressures of 250, 750, and 1000 mbar (absolute pressure). The samples were heated from room temperature to 500 °C at a rate of 50 °C/s and held at 500 °C for 1 min. Following pyrolysis, the glass housing tube was washed with methanol to collect condensed products for further (offline) analysis by electrospray ionization (ESI)-FT-ICR MS (9.4 T Bruker Solarix) in the positive ion mode. The collected FT-ICR MS spectra were further compiled and assigned with the Composer software (Sierra Analytics). A complete description of the experimental pyrolysis details and results are available in the previously published study by Pecha et al.⁵¹ The emphasis of this work is primarily centered on the analysis of the pyrolysis product ESI-FT-ICR MS results as they relate to lignin characterization MALDI-FT-ICR MS results.

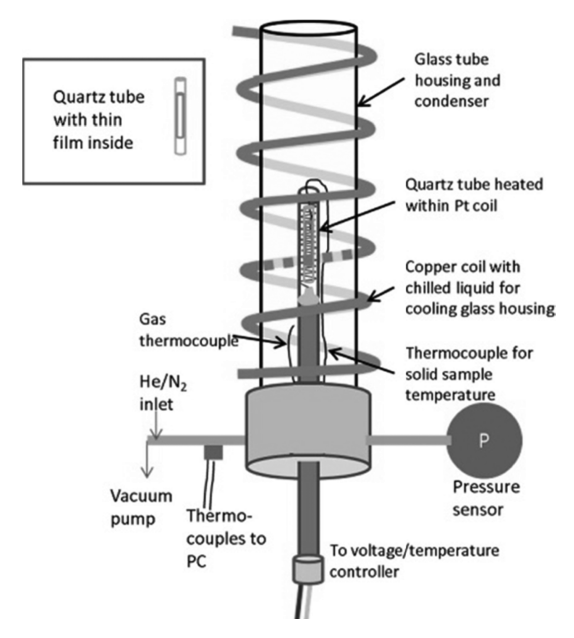


Figure 1. Illustration of the modified pyroprobe reactor for experimental pyrolysis. Reproduced from Pecha et al.⁵¹

2.4. Strategy for Oligomeric Lignin Product Structure Assignment. Structure representations were proposed for high-abundance FT-ICR MS-detected products based on the combinatoric expansion of chemical formulas from raw MWL, for which structures were previously proposed.³⁰ The top 25 trimers and top 10 tetramers for each sample were assigned to suggested structures. Raw MWL chemical formulas were expanded based on the consideration of the changes in hydrogen, methyl, and hydroxyl groups; these groups can be

used to represent all of the fragmentation reactions employed in the coupled structural and kinetic model from Yanez et al., for example.⁴⁵ All possible combinations of -2, -1, ± 0 , +1, +2 H₂, CH₃, and OH were applied to oligomers of raw MWL, producing 7000 modified formulas from an original set of 30 trimers and 30 tetramers.

2.5. Lignin Vacuum Pyrolysis Model. To highlight the effect of pressure on the molecular weight of lignin pyrolysis products, an integrated model using stochastic/probabilistic parameters was developed. A figure showing an overview of the algorithm and further details describing the model parameters are given in the Supporting Information. Initially, lignin is modeled as a truncated lognormal distribution swith degree of polymerization between 2 and a user-defined upper limit. Each of the individual entries in the starting distribution is then parameterized by a labile bond propensity, which randomly assigns and breaks interunit linkages in an individual polymer entry. Following this depolymerization, a fraction of the resulting depolymerized units recombines according to a recombination propensity, estimated based on pyrolysis/carbonization kinetics (and therefore, temperature).

Once each entry in the starting lognormal distribution undergoes depolymerization and recombination, it is stored in a collection of "initial pyrolysis products." This collection of initial products is then partitioned into oil and char precursors based on mass transport phenomena. The model features two for-loops. The first loop populates "initial pyrolysis products" based on the depolymerization and recombination of the starting lognormal distribution. The second loop populates "final products" based on the partitioning of the initial products according to evaporation and aerosol ejection into "oil" and "char precursor." If the vaporization temperature for a given entry is less than the reaction temperature, it is collected

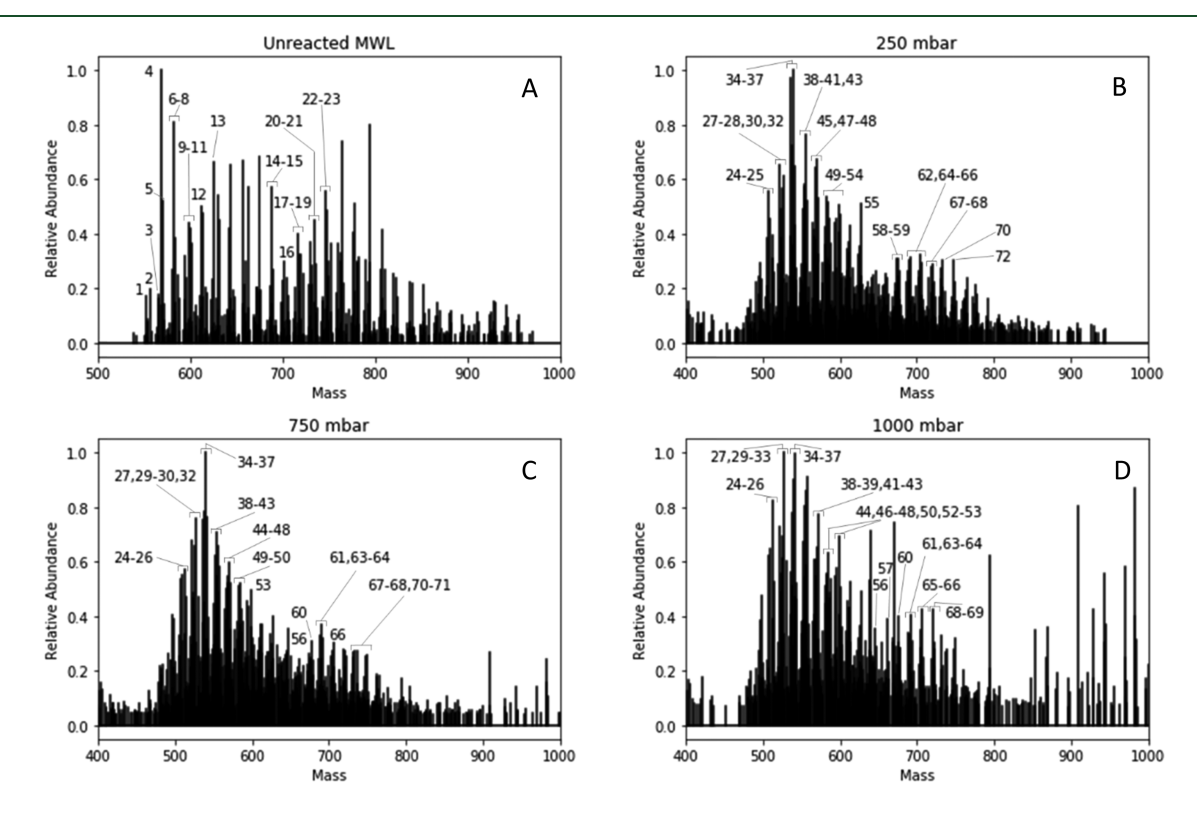


Figure 2. Representations of the FT ICR mass spectra for (A) unreacted MWL and the pyrolysis products from reaction at (B) 250 mbar, (C) 750 mbar, and (D) 1000 mbar. Numbered peaks correspond to pathways/structures provided in Tables 1–4.

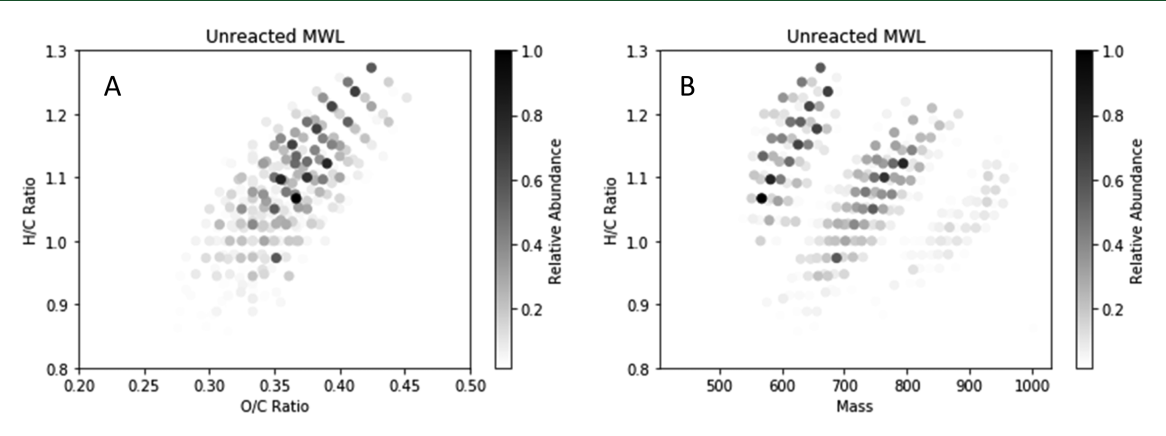


Figure 3. Plots of MWL showing the (A) van Krevelen diagram and (B) H/C ratio vs mass, adapted from Terrell et al. 30

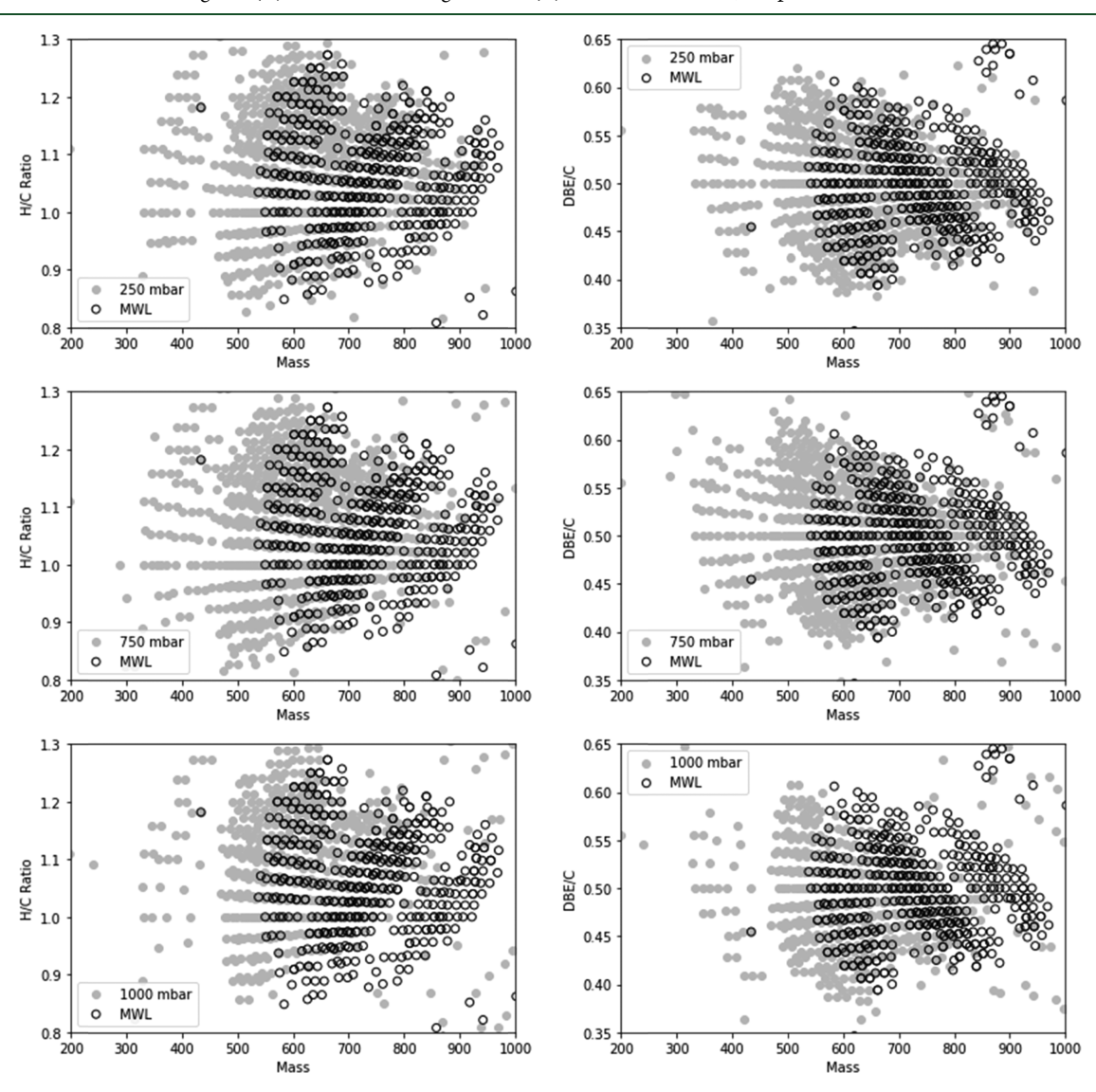


Figure 4. Comparisons of the H/C ratio and DBE/C value vs mass between unreacted MWL and its pyrolysis products. The pyrolysis pressures are given in the legend of each plot, and the y-axes correspond to H/C ratios (left plots) and DBE/C values (right plots).

as oil; if the vaporization temperature is greater than the reaction temperature, it is collected as the char precursor. A random fraction of the char precursor entries is reassigned as an oil entry based on aerosol ejection propensity. ⁶⁰ Finally, the char precursors are partitioned into char, water, and gas based on a stoichiometric relationship. ⁴⁵ The reported data include

the yields of monomers, oligomers, and char, as well as the molecular weight of the initial lignin and modeled lignin pyrolysis oil. The model data are compared with the experimental results reported by Pecha et al. and Marathe et al. 44,51

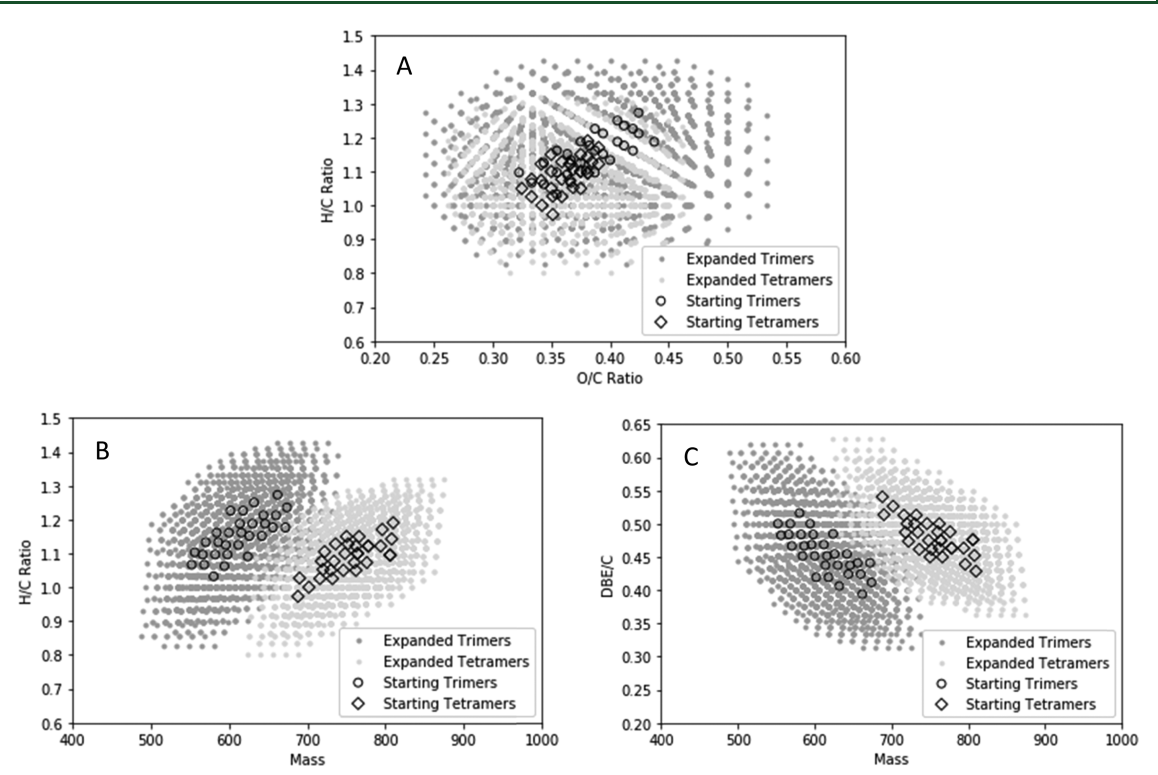


Figure 5. Expansion of values for unreacted MWL trimers and tetramers, showing the (A) van Krevelen diagram, (B) H/C ratio vs mass, and (C) DBE/C value vs mass.

3. RESULTS AND DISCUSSION

3.1. FT-ICR MS Results and Data Visualization. The representations of the mass spectrum are given in Figure 2 for the raw MWL and reaction products at 250, 750, and 1000 mbar. The x-axis label corresponds to the nominal mass calculated from the $C_xH_yO_z$ formula assigned to each peak. The numbers on the spectra denote oligomeric peaks for which a structure assignment is proposed. Raw MWL is labeled with numbers 1-23, and the pyrolysis products are labeled with 24-72. Many pyrolysis products share common abundant oligomers.

The representations of raw MWL MS characterization are given in Figure 3, which features a van Krevelen diagram and a plot of H/C ratio versus mass. The van Krevelen diagram is useful for segregating between different molecular classes (e.g., cellulose, lignin, protein, lipids, and condensed hydrocarbons) and for highlighting potential reaction pathways. 50,61 The H/C ratio versus mass plot has utility in its ability to highlight lignin clusters with different numbers of aromatic rings.³⁰ Due to its well-preserved aromatic structure, detected lignin molecules reside within a relatively constant H/C range (viz., H/C \approx 0.9-1.2); however, due to its polymeric nature, the same lignin molecules fall within more discretized mass groups (viz., mass \approx 500-600, 650-750, and 800-950; trimers, tetramers, and pentamers, respectively). Although certain mass features can be elucidated, the nature of ionization and ion transfer (which must be optimized for a given analysis) within an FT-ICR MS instrument provides only a semiquantitative measure of the molecular weight distribution of the measured sample. Different ionization modes and conditions applied to the same sample can yield different molecular weight distribution results. 28,62

The same plots (i.e., van Krevelen diagram and H/C ratio vs mass) are given for lignin pyrolysis products in the Supporting

Information. In general, these plots share many of the same characteristics as those for raw MWL, confirming that there is a reasonable similarity among the samples. The points on the van Krevelen diagram for pyrolysis cover a wider range of O/C and H/C values. The detected pyrolysis products also have a more limited number of detected ions in the pentamer mass range (mass $\approx 800-950$) and a set of low abundance points in the dimer mass range (mass $\approx 300-400$) not present in raw MWL.

In addition to Figure S2, which highlights the FT-ICR MS intensity of the plotted peaks, Figure 4 depicts the plots of the H/C ratio vs mass and the carbon-normalized double bond equivalent (DBE/C) value vs mass for each pyrolysis sample in combination with raw MWL. The DBE/C value (eq 1) has been reported to be a useful measure of aromaticity, as described by Hockaday et al., in studies that utilize FT-ICR MS for soil characterization. In general, the DBE/C value tends to decrease with an increase in aliphatic moieties (e.g., phenol > guaiacol > coniferyl alcohol > sinapyl alcohol). The DBE/C value is algebraically similar to the H/C ratio; therefore, the plots of DBE/C and H/C vs mass share similar features.

$$\frac{DBE}{C} = \frac{\left(C + 1 - \frac{H}{2}\right)}{C} = 1 + \frac{1}{C} - \frac{1}{2} \times \frac{H}{C}$$
 (1)

3.2. Structural Proposal for Lignin Oligomers. For raw MWL, structural representations were proposed for peaks with high abundance among the detected trimers, tetramers, and pentamers (shown elsewhere).³⁰ These proposals/assignments were made based on coupling analytical characterization data with the stochastic modeling of the lignin structure.³⁰ These assignments are used here to propose similar structural representations for the detected pyrolysis product peaks with

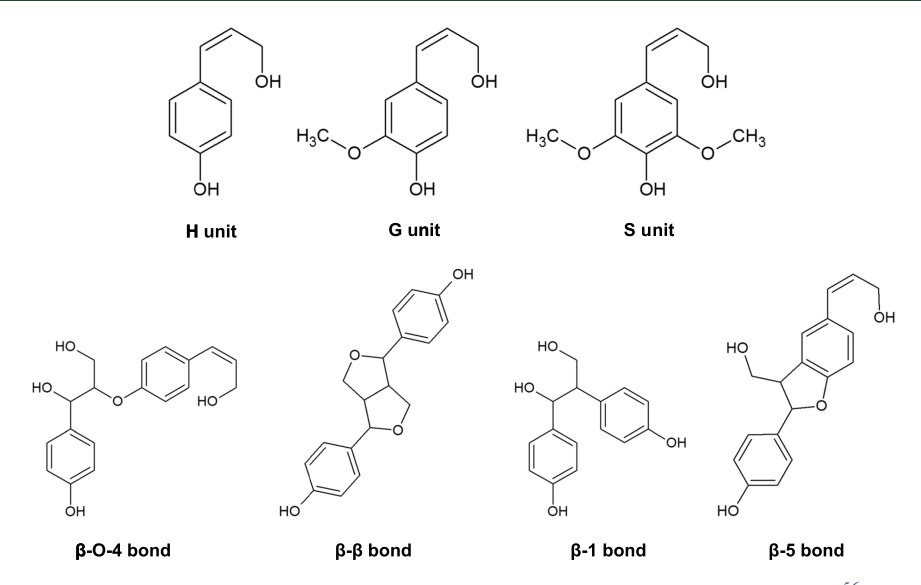
Table 1. Selection of Proposed Assignments for MWL Oligomers³⁰

no. (trimer/tetramer)	formula	nom. mass	assignment	
1 – trimer	$C_{30}H_{32}O_{10}$	552	S (β O4) H (β 5) G – H ₂	
			$G(\beta\beta) G(\beta O4) G - H_2$	
2 – trimer	$C_{29}H_{32}O_{11}$	556	S (β 5) G (β O4) G – 2CH ₃	
			G (β O4) G (β O4) G – CH ₃ – H ₂	
3 – trimer	$C_{31}H_{34}O_{10}$	566	G (β 5) G (β O4) S – CH ₃ – H ₂	
			$S (\beta 5) G (\beta O4) S - OH - 2CH_3 - H_2$	
4 – trimer	$C_{30}H_{32}O_{11}$	568	G (β O4) G (β O4) G – 2H ₂	
			$S (\beta O4) G (\beta O4) H - 2H_2$	
5 – trimer	$C_{30}H_{34}O_{11}$	570	G (β O4) G (β O4) G – H ₂	
			S (β O4) G (β O4) H – H ₂	
6 – trimer	$C_{31}H_{34}O_{11}$	582	$H (\beta O4) S (\beta O4) S - OH - 2H_2$	
			G (β O4) G (β O4) S – OH – 2H ₂	
7 – trimer	$C_{31}H_{36}O_{11}$	584	$H (\beta O4) S (\beta O4) S - OH - H_2$	
			G (β O4) G (β O4) S – OH – H ₂	
8 – trimer	$C_{30}H_{34}O_{12}$	586	$S(\beta O4) S(\beta S) G - 2CH_3$	
			$S(\beta\beta) G(\betaO4) S - 2CH_3$	
9 – trimer	$C_{32}H_{36}O_{11}$	596	G (β O4) G (β O4) S – 2H ₂	
			$S(\beta\beta) G(\betaO4) S - OH - H_2$	
10 - trimer	$C_{31}H_{36}O_{12}$	600	$H (\beta O4) S (\beta O4) S - H_2$	
			$G(\beta O4) G(\beta O4) S - H_2$	
11 – trimer	$C_{31}H_{38}O_{12}$	602	Η (βO4) S (βO4) S	
	0- 0		$G(\beta O4) G(\beta O4) S$	
12 – trimer	$C_{32}H_{38}O_{12}$	614	$S(\beta\beta) G(\betaO4) S$	
			$S(\beta S) G(\beta O 4) S$	
13 - trimer	$C_{33}H_{38}O_{12}$	626	$S(\beta O4) S(\beta \beta) S - OH - H_2$	
	33 30 12		$S(\beta O4) S(\beta O4) S - 2OH - 2H_2$	
14 – tetramer	$C_{37}H_{36}O_{13}$	688	$G(\beta 5) H(\beta O4) S(\beta 1) G - 3H_2$	
	0, 0, 10		$G(\beta O4) G(\beta 1) G(\beta O4) G - OH - 4H_2$	
15 – tetramer	$C_{37}H_{38}O_{13}$	690	G (β 5) H (β O4) S (β 1) G – 2H ₂	
			$S(\beta 1) G(\beta O4) G(\beta O4) H - OH - 3H_2$	
16 – tetramer	$C_{38}H_{38}O_{13}$	702	H (β O4) G (β O4) G (β O4) H – 3H ₂	
	0. 00 10		$S (\beta O4) H (\beta 1) S (\beta O4) G - 2OH - 4H_2$	
17 – tetramer	$C_{39}H_{42}O_{13}$	718	G $(\beta\beta)$ S $(\betaO4)$ H $(\betaO4)$ H $-$ H ₂	
	0, 12 10		S (β O4) H (β O4) H (β O4) G – OH – 2H ₂	
18 – tetramer	$C_{38}H_{40}O_{14}$	720	G (β O4) G (β O4) G (β O4) G – OH – 2CH ₃ – 2H	
	0- 10 11		G (β 1) S (β O4) G (β O4) G – OH – 3H ₂	
19 – tetramer	$C_{38}H_{42}O_{14}$	722	G (β O4) G (β O4) G (β O4) H – CH ₃ – H ₂	
	JU 72 17		S (β O4) H (β 1) S (β O4) G – OH – 2H ₂	
20 – tetramer	$C_{39}H_{42}O_{14}$	734	S (β O4) H (β O4) H (β O4) G – 2H ₂	
	J) #2 - 1#		H (β O4) G (β O4) G (β O4) G -2 H ₂	
21 – tetramer	$C_{39}H_{44}O_{14}$	736	G (β O4) G (β O4) G (β O4) H – H ₂	
	J/ 44 - 14		G $(\beta\beta)$ S $(\beta O4)$ G $(\beta O4)$ H – CH ₃	
22 – tetramer	$C_{40}H_{44}O_{14}$	748	G $(\beta\beta)$ S $(\beta O4)$ G (βS) G – CH ₃	
	- 40 - 44 - 14		H (β O4) S (β O4) G (β O4) G – OH – 2H ₂	
23 – tetramer	$C_{40}H_{46}O_{14}$	750	S $(\beta\beta)$ G $(\beta O4)$ H $(\beta O4)$ G	
	-4040 × 14	. 50	$G(\beta S) G(\beta O A) G(\beta O A) G$	

high MS abundance, based on the combinatoric expansion of raw MWL chemical formulas. In particular, the top 25 trimers and top 10 tetramers from each presented reaction pressure (i.e., 250, 750, and 1000 mbar) are assigned. The results from the combinatoric expansion of raw MWL oligomers is shown in Figure 5 as a van Krevelen diagram and plots of H/C ratio and DBE/C vs mass.

Table 1 shows a selection of raw MWL oligomers that are used as a basis for pyrolysis oligomer assignments. These assignments are not necessarily unique, and other possibilities are certainly imaginable. An H, G, and/or S represents the monomer unit in the proposed oligomer (H = p-hydroxyphenyl, G = guaiacyl, and S = syringyl), and the

bond type connecting two monomers is denoted in parentheses (following the convention shown by Dellon et al. for lignin structure simulation, as shown in Figure 6). Only the relative compositions of β -bond types were determined in the original work for the lignin oligomer structure assignment. Tables 2–4 show the proposed structural assignments for pyrolysis oligomers from reactions at 250, 750, and 1000 mbar, respectively. A specified loss of a hydroxyl group is equivalent to the loss of one oxygen from the $C_xH_yO_z$ formula; similarly, the loss of a methyl group corresponds to one carbon and two hydrogens. These pyrolysis product assignments (Tables 2–4) are reported as modifications of the raw MWL oligomers in Table 1.



 $\textbf{Figure 6.} \ \ \text{Naming and structure convention for the lignin monomer and bond types, adapted from Dellon et al.}^{56}$

Table 2. Proposed Assignments for 250 mbar Pyrolysis Oligomers as Modifications of MWL

no. (trimer/tetramer)	relative abundance	formula	nom. mass	assignment ^a
24 – trimer	0.557	$C_{28}H_{28}O_9$	508	$[2] - 2OH - CH_3 - H_2$
25 – trimer	0.455	$C_{28}H_{30}O_9$	510	$[1] - OH - 2CH_3 + H_2$
27 – trimer	0.653	$C_{29}H_{30}O_{9}$	522	$[1] - OH - CH_3$
28 - trimer	0.490	$C_{28}H_{28}O_{10}$	524	$[1] - 2CH_3$
30 – trimer	0.564	$C_{28}H_{30}O_{10}$	526	$[2] - OH - CH_3$
32 – trimer	0.610	$C_{28}H_{32}O_{10}$	528	$[2] - OH - CH_3 + H_2$
34 – trimer	0.972	$C_{29}H_{28}O_{10}$	536	$[4] - OH - CH_3 - H_2$
35 – trimer	0.723	$C_{29}H_{30}O_{10}$	538	$[2] - OH - H_2$
36 – trimer	1.000	$C_{29}H_{32}O_{10}$	540	[2] - OH
37 – trimer	0.647	$C_{29}H_{34}O_{10}$	542	$[2] - OH + H_2$
38 - trimer	0.489	$C_{30}H_{32}O_{10}$	552	[1]
39 - trimer	0.579	$C_{30}H_{34}O_{10}$	554	[5] - OH
40 – trimer	0.572	$C_{29}H_{30}O_{11}$	554	$[2] - H_2$
41 – trimer	0.764	$C_{29}H_{32}O_{11}$	556	[2]
43 – trimer	0.523	$C_{29}H_{34}O_{11}$	558	$[2] + H_2$
45 – trimer	0.644	$C_{30}H_{32}O_{11}$	568	[4]
47 – trimer	0.674	$C_{30}H_{34}O_{11}$	570	[5]
48 – trimer	0.531	$C_{30}H_{36}O_{11}$	572	$[5] + H_2$
49 – trimer	0.536	$C_{31}H_{34}O_{11}$	582	[6]
50 - trimer	0.515	$C_{31}H_{36}O_{11}$	584	[7]
51 – trimer	0.455	$C_{30}H_{34}O_{12}$	586	[8]
52 – trimer	0.455	$C_{32}H_{36}O_{11}$	596	[9]
53 – trimer	0.506	$C_{32}H_{38}O_{11}$	598	[12] - OH
54 – trimer	0.471	$C_{31}H_{36}O_{12}$	600	[10]
55 – trimer	0.510	$C_{33}H_{40}O_{12}$	628	$[13] + H_2$
58 - tetramer	0.307	$C_{37}H_{38}O_{12}$	674	[15] - OH
59 – tetramer	0.308	$C_{37}H_{40}O_{12}$	676	$[15] - OH + H_2$
62 – tetramer	0.301	$C_{37}H_{38}O_{13}$	690	[15]
64 – tetramer	0.313	$C_{37}H_{40}O_{13}$	692	$[14] + 2H_2$
65 – tetramer	0.325	$C_{38}H_{40}O_{13}$	704	[18] - OH
66 – tetramer	0.294	$C_{38}H_{42}O_{13}$	706	$[23] - OH - 2CH_3$
67 – tetramer	0.277	$C_{39}H_{42}O_{13}$	718	$[21] - OH - H_2$
68 – tetramer	0.288	$C_{39}H_{42}O_{13}$	720	$[17] + H_2$
70 – tetramer	0.303	$C_{39}H_{42}O_{14}$	734	[20]
72 – tetramer	0.301	$C_{40}H_{44}O_{14}$	748	[22]

3.3. Analysis of Proposed Oligomer Formulas. For each $C_xH_vO_z$ formula in Tables 2–4, the nominal mass, H/C

ratio, and DBE/C value are calculated, along with the same values for the top 25 trimers and top 10 tetramers from raw

Table 3. Proposed Assignments for 750 mbar Pyrolysis Oligomers as Modifications of MWL

no. (trimer/tetramer)	relative abundance	formula	nom. mass	assignment ^a
24 – trimer	0.538	$C_{28}H_{28}O_9$	508	$[2] - 2OH - CH_3 - H_2$
25 – trimer	0.549	$C_{28}H_{30}O_{9}$	510	$[1] - OH - 2CH_3 + H_2$
26 – trimer	0.572	$C_{28}H_{32}O_{9}$	512	$[2] - 2OH - CH_3 + H_2$
27 – trimer	0.678	$C_{29}H_{30}O_{9}$	522	$[1] - OH - CH_3$
29 – trimer	0.486	$C_{29}H_{32}O_{9}$	524	[2] - 2OH
30 – trimer	0.655	$C_{28}H_{30}O_{10}$	526	$[2] - OH - CH_3$
32 – trimer	0.759	$C_{28}H_{32}O_{10}$	528	$[2] - OH - CH_3 + H_2$
34 – trimer	0.752	$C_{29}H_{28}O_{10}$	536	$[4] - OH - CH_3 - H_2$
35 – trimer	0.782	$C_{29}H_{30}O_{10}$	538	$[2] - OH - H_2$
36 – trimer	1.000	$C_{29}H_{32}O_{10}$	540	[2] - OH
37 – trimer	0.760	$C_{29}H_{34}O_{10}$	542	$[2] - OH + H_2$
38 – trimer	0.624	$C_{30}H_{32}O_{10}$	552	[1]
39 – trimer	0.707	$C_{30}H_{34}O_{10}$	554	[5] - OH
40 – trimer	0.548	$C_{29}H_{30}O_{11}$	554	$[2] - H_2$
41 – trimer	0.660	$C_{29}H_{32}O_{11}$	556	[2]
42 – trimer	0.486	$C_{30}H_{36}O_{10}$	556	$[11] - 2OH - CH_3$
43 – trimer	0.581	$C_{29}H_{34}O_{11}$	558	$[2] + H_2$
44 – trimer	0.501	$C_{31}H_{34}O_{10}$	566	[3]
45 – trimer	0.544	$C_{30}H_{32}O_{11}$	568	[4]
46 – trimer	0.519	$C_{31}H_{36}O_{10}$	568	[7] - OH
47 – trimer	0.597	$C_{30}H_{34}O_{11}$	570	[5]
48 – trimer	0.519	$C_{30}H_{36}O_{11}$	572	$[5] + H_2$
49 – trimer	0.511	$C_{31}H_{34}O_{11}$	582	[6]
50 – trimer	0.519	$C_{31}H_{36}O_{11}$	584	[7]
53 – trimer	0.497	$C_{32}H_{38}O_{11}$	598	[12] - OH
56 – tetramer	0.275	$C_{36}H_{38}O_{11}$	646	$[15] - 2OH - CH_3 + H_3$
60 – tetramer	0.306	$C_{36}H_{38}O_{13}$	678	$[15] - CH_3 + H_2$
61 – tetramer	0.327	$C_{38}H_{40}O_{12}$	688	$[16] - OH + H_2$
63 – tetramer	0.367	$C_{38}H_{42}O_{12}$	690	[19] - 2OH
64 – tetramer	0.320	$C_{37}H_{40}O_{13}$	692	$[14] + 2H_2$
66 – tetramer	0.306	$C_{38}H_{42}O_{13}$	706	$[23] - OH - 2CH_3$
67 – tetramer	0.277	$C_{38}H_{42}O_{13}$	718	$[21] - OH - H_2$
68 – tetramer	0.273	$C_{39}H_{44}O_{13}$	720	$[17] + H_2$
70 – tetramer	0.274	$C_{39}H_{42}O_{14}$	734	[20]
71 – tetramer	0.274	$C_{39}H_{44}O_{14}$	736	$[20] + H_2$

^aBracketed number corresponds to the numbered entry in Table 1.

MWL. These metrics, which are shown in Figure 7, are then used as a basis for statistical analysis ($\alpha = 0.05$) to compare raw MWL to its pyrolysis oligomers. Further details of the analysis are given in the Supporting Information. Only the top 25 trimers and top 10 tetramers from each data set (i.e., raw MWL, 250, 750, and 1000 mbar) are considered, with the assumption that these most abundant FT-ICR MS peaks are reasonable surrogates for the whole sample.

There is a significant difference in the molecular weight and O/C ratio between raw MWL and its pyrolysis products (i.e., 250, 750, and 1000 mbar) for both abundant trimers and tetramers. Additionally, there is a significant difference between raw MWL and its pyrolysis products for H/C ratio (with the exception of 1000 mbar for H/C) and DBE/C with respect to abundant trimers, but the difference is not significant for abundant tetramers. In general, the differences between molecular weight, O/C ratio, H/C ratio, and DBE/C among the pyrolysis product sets tend to be not significant, most likely due to the prevalence of shared oligomers among the reaction samples. This analysis suggests that during pyrolysis, lignin oligomers experience a decrease in the molecular weight and O/C ratio. The average analyzed molecular weights are 620, 550, 720, and 700 for raw MWL trimers, pyrolysis trimers, raw

MWL tetramers, and pyrolysis tetramers, respectively. The average analyzed O/C ratios are 0.38, 0.35, 0.36, and 0.34 for raw MWL trimers, pyrolysis trimers, raw MWL tetramers, and pyrolysis tetramers, respectively. Pyrolytic evolution toward lighter molecules is observable in Figure 4.

3.4. Estimation of Normal Boiling Point for Lignin **Oligomers.** To assess further the hypothesis regarding direct oligomer vaporization, a set of empirical correlations were used to determine the normal boiling point (T_{nb}) for representative monomers and oligomers. The correlations represent $T_{\rm nb}$ (°C) as various functions of molecular weight and carbon number (additional details in the Supporting Information). 64-69 Calculations were carried out using the temperature units specified in a given source as is and then converted to degree Celsius for use herein. These correlations were applied to monomers of p-coumaryl alcohol (H-unit), coniferyl alcohol (G-unit), and sinapyl alcohol (S unit) and their respective β -O-4-connected dimers, trimmers, and tetramers. Regression analysis was then applied to the resulting set of $T_{\rm nb}$ values plotted against the molecular weight and carbon number, as shown in Figure 8. The 95% confidence interval and 95% prediction intervals are also shown. The linear regressions for Figure 8 are given in eqs 2 and 3 (where MW = molecular

Table 4. Proposed Assignments for 1000 mbar Pyrolysis Oligomers as Modifications of MWL

no. (trimer/tetramer)	relative abundance	formula	nom. mass	assignment ^a
24 – trimer	0.620	$C_{28}H_{28}O_9$	508	$[2] - 2OH - CH_3 - H_2$
25 – trimer	0.649	$C_{28}H_{30}O_{9}$	510	$[1] - OH - 2CH_3 + H_2$
26 – trimer	0.825	$C_{28}H_{32}O_9$	512	$[2] - 2OH - CH_3 + H_2$
27 - trimer	0.730	$C_{29}H_{30}O_{9}$	522	$[1] - OH - CH_3$
29 - trimer	0.558	$C_{29}H_{32}O_{9}$	524	[2] - 2OH
30 - trimer	0.693	$C_{28}H_{30}O_{10}$	526	$[2] - OH - CH_3$
31 – trimer	0.610	$C_{29}H_{34}O_{9}$	526	$[2] - 2OH + H_2$
32 – trimer	1.000	$C_{28}H_{32}O_{10}$	528	$[2] - OH - CH_3 + H_2$
33 – trimer	0.603	$C_{28}H_{34}O_{10}$	530	$[5] - OH - 2CH_3 + 2H_3$
34 - trimer	0.563	$C_{29}H_{28}O_{10}$	536	$[4] - OH - CH_3 - H_2$
35 – trimer	0.777	$C_{29}H_{30}O_{10}$	538	$[2] - OH - H_2$
36 – trimer	0.901	$C_{29}H_{32}O_{10}$	540	[2] - OH
37 – trimer	0.996	$C_{29}H_{34}O_{10}$	542	$[2] - OH + H_2$
38 - trimer	0.673	$C_{30}H_{32}O_{10}$	552	[1]
39 – trimer	0.802	$C_{30}H_{34}O_{10}$	554	[5] - OH
41 – trimer	0.857	$C_{29}H_{32}O_{11}$	556	[2]
42 – trimer	0.589	$C_{30}H_{36}O_{10}$	556	$[11] - 2OH - CH_3$
43 – trimer	0.909	$C_{29}H_{34}O_{11}$	558	$[2] + H_2$
44 – trimer	0.608	$C_{31}H_{34}O_{10}$	566	[3]
46 – trimer	0.607	$C_{31}H_{36}O_{10}$	568	[7] - OH
47 – trimer	0.654	$C_{30}H_{34}O_{11}$	570	[5]
48 - trimer	0.774	$C_{30}H_{36}O_{11}$	572	$[5] + H_2$
50 - trimer	0.630	$C_{31}H_{36}O_{11}$	584	[7]
52 - trimer	0.575	$C_{32}H_{36}O_{11}$	596	[9]
53 - trimer	0.692	$C_{32}H_{38}O_{11}$	598	[12] - OH
56 – tetramer	0.356	$C_{36}H_{38}O_{11}$	646	$[15] - 2OH - CH_3 + H_3$
57 – tetramer	0.390	$C_{36}H_{38}O_{12}$	662	$[15] - OH - CH_3 + H_2$
60 – tetramer	0.399	$C_{37}H_{40}O_{12}$	676	$[15] - OH + H_2$
61 – tetramer	0.339	$C_{38}H_{40}O_{12}$	688	$[16] - OH + H_2$
63 – tetramer	0.332	$C_{38}H_{42}O_{12}$	690	[19] - 2OH
64 – tetramer	0.404	$C_{37}H_{40}O_{13}$	692	$[14] + 2H_2$
65 – tetramer	0.349	$C_{38}H_{40}O_{13}$	704	[18] - OH
66 – tetramer	0.424	$C_{38}H_{42}O_{13}$	706	$[23] - OH - 2CH_3$
68 – tetramer	0.423	$C_{39}H_{44}O_{13}$	720	$[17] + H_2$
69 – tetramer	0.329	$C_{40}H_{44}O_{13}$	732	[22] - OH

^aBracketed number corresponds to the numbered entry in Table 1.

weight and C# = carbon number). In reality, thermochemical/physical property (e.g., $T_{\rm nb}$, heat of vaporization, and solubility parameters) prediction is much more complicated than a simple linear regression of one variable; $^{70-72}$ however, we propose that the presented analysis is a useful semiquantitative tool for observing general trends regarding $T_{\rm nb}$. Physical and/or chemical interpretations of the coefficient and intercept values may be obfuscated by reducing complex phenomena, such as liquid boiling, to a regression equation of one variable. The molecular size and the tendency for intermolecular interactions (especially H-bonding) are known to have a strong effect on the boiling point of a liquid compound or mixture.

$$T_{\rm nb}$$
 (°C) = 0.686*MW + 138 (R^2 = 0.78) (2)

$$T_{\rm ph}$$
 (°C) = 12.7*C# + 127 ($R^2 = 0.79$) (3)

The pyrolysis of MWL studied in this work was carried out at a reactor temperature of 500 °C. Based on the confidence intervals in Figure 8, an estimated $T_{\rm nb}$ value of 500 °C corresponds approximately to a molecular weight of 530 \pm 30 and a carbon number of 29 \pm 2. The prediction intervals contain, naturally, a much larger range of molecular weights and carbon numbers. This result suggests that at 500 °C (and

1 bar), it is possible for molecules with mass from \sim 500 to 560 Da and carbon number from \sim 27 to 31 to vaporize directly. For lignin specifically, this range primarily contains trimers. Smaller molecules are also capable of vaporization under these conditions. This is consistent with the reported experimental results of the molecular weight of lignin pyrolysis oils resulting from different reactor pressures. 44

The most abundant oligomers resulting from pyrolysis studied here are trimers, with a lesser quantity of tetramers. Operation at a lower reactor pressure results in a decrease in the vaporization temperature (via Clausius—Clapeyron relation, eq 4), which may encourage the vaporization of heavier lignin oligomers. Additionally, it is also probable that heavy oligomers may be collected as primary products due to aerosol ejection phenomena that have been shown to exist during lignin pyrolysis. 73,74

$$\ln\left(\frac{P_2}{P_1}\right) = -\frac{\Delta H_{\text{vap}}}{R} \left(\frac{1}{T_2} - \frac{1}{T_1}\right) \tag{4}$$

Due to the lack of a true structural/conformational analysis of MWL and its pyrolysis products (for example, with density functional theory), it is not currently possible here to achieve

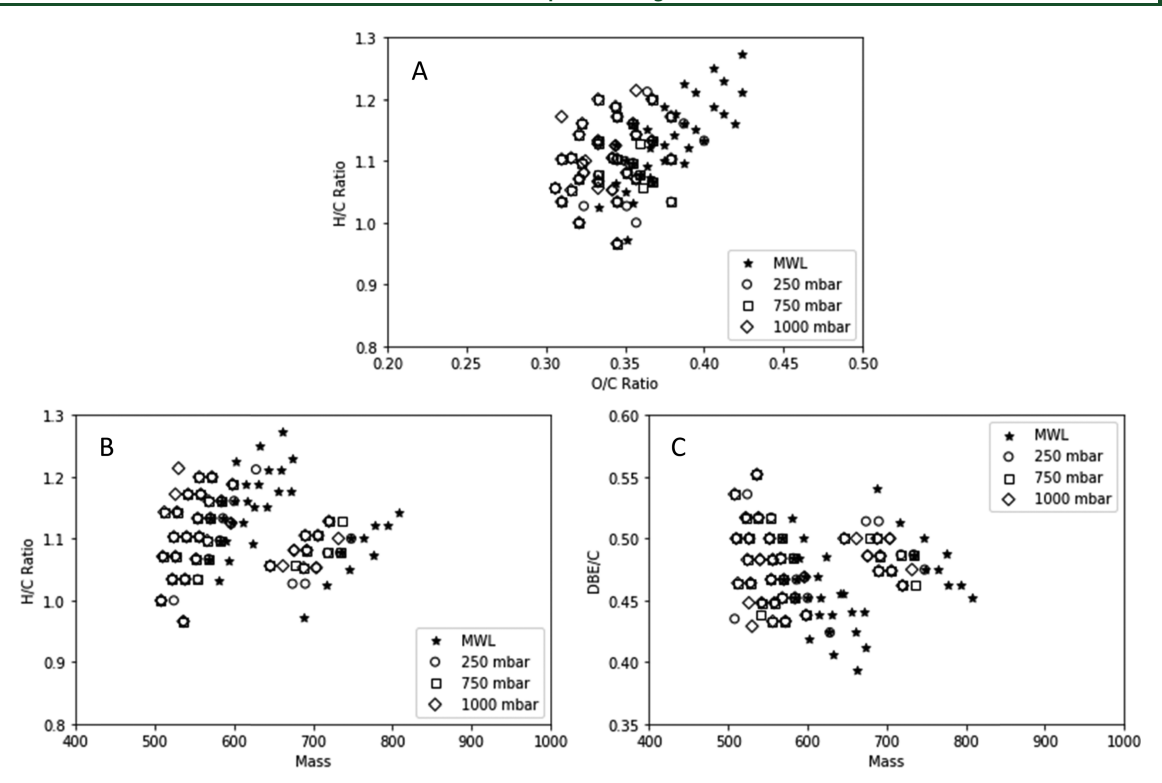


Figure 7. Plots of the (A) van Krevelen diagram, (B) H/C ratio vs mass, and (C) DBE/C value vs mass for assigned trimers and tetramers in Tables 1-4.

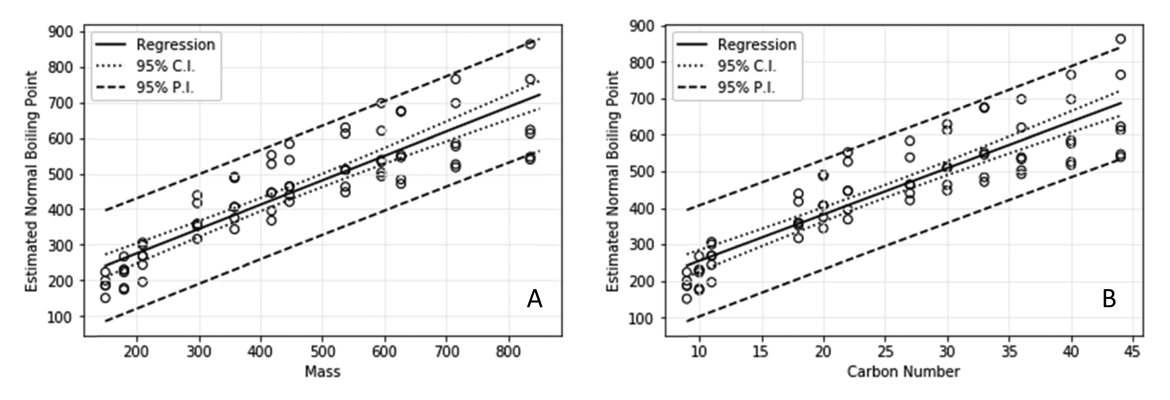


Figure 8. Linear regression of empirical boiling point ($^{\circ}$ C) correlations with 95% confidence and prediction intervals (C.I. and P.I., respectively) for (A) mass and (B) C#.

robust quantitative structure—property relationships. Group contribution methods have been suggested previously to estimate vaporization curves for lignin oligomers. ⁴⁷ A point of emphasis for future work can be to develop more rigorous structural analysis, which can then be employed as the basis for calculating more accurate thermophysical/chemical properties. Nevertheless, one potential approach for these calculations is to use an empirical correlation (modified Trouton's rule) between the entropy of vaporization ($\Delta S_{\rm vap}$) and $T_{\rm nb}$ to estimate the enthalpy of vaporization ($\Delta H_{\rm vap}$). ⁷⁵ These thermochemical values can then be used in the Clausius—Clapeyron relation (eq 4) to determine the vaporization temperature at a lowered pressure.

Based on this analysis for tetramers (mass of \sim 700 Da, C# of \sim 40), the estimated $\Delta H_{\rm vap}$ is 80–85 kJ/mol, resulting in a boiling point at 250 mbar of 500–550 °C. Further calculation details are given in the Supporting Information. This result suggests that for a pyrolysis temperature of approximately 500

°C, it is distinctly possible for tetramers (and smaller species) to directly evaporate at pressures of 250 mbar and lower. Experimental evidence of tetramers at higher pressures may be the result of aerosol ejection or secondary recombination phenomena. 40,51,76 For FT-ICR MS measurements specifically, ionization and/or ion transfer effects are also important. Extending this analysis of thermophysical/chemical properties to any arbitrary temperature and pressure combination allows for estimation, albeit with reasonably large uncertainty, of the size of oligomeric species that can achieve direct vaporization during pyrolysis. In this way, pressure is shown to have an important impact on the pyrolysis process. Although pressure has no theoretical effect on the reaction kinetics of solid and liquid phases, it is still important in governing mass transport phenomena. The pressure of a pyrolysis reactor therefore has an important effect on the molecular weight of pyrolysis products.

3.5. Lignin Vacuum Pyrolysis Model. The results from pyrolysis modeling in comparison with the results reported by Pecha et al.⁵¹ are given in Table 5. The model is described in

Table 5. Comparison between Modeled and Reported Experimental Results for Lignin Pyrolysis

pressure (mbar)	monomer yield (model)	oligomer yield (model)	Char yield (model)	Char yield (Pecha et al. ⁵¹)
250	5.06	41.5	22.6	24.3
750	5.05	23.7	33.0	35.3
1000	5.08	22.2	33.8	35.6

greater detail in the Supporting Information. A value of 0.45 was used for the labile bond propensity, based on the estimation of the β -O-4 content of hardwood MWL, which also shows reasonably good correspondence with the reported experimental char values. The estimated recombination propensity for 500 °C is 0.88 (details are provided in the Supporting Information). The aerosol propensity was set to 0.1 for 250 mbar, 0.08 for 750 mbar, and 0.05 for 1000 mbar, estimated based on the previous work on pyrolysis oligomers and aerosols. A fixed model molecular weight of ~2000 Da was also used for this specific comparison. At a model pressure of 250 mbar, monomers, dimers, trimers, and tetramers were allowed to evaporate. At 750 and 1000 mbar, only monomers, dimers, and trimers were allowed to evaporate.

The modeled char yields show good agreement across the reported experimental pressure range. At low pressure, there is less char resulting from a greater extent of evaporation of high-molecular weight species. This is also mirrored by the inverse relationship between the oligomer and char yields in both the model results and semiquantitative experimental results from UV-fluorescence analysis. 51,79 Pressure has virtually no effect on monomer yields, which is also shown experimentally by Pecha et al., who report constant total monomer yields of roughly 2–3%. 51

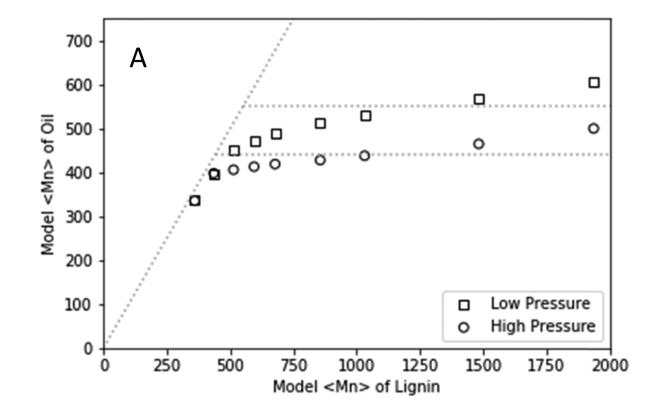
To further assess the presented modeling approach, oil molecular weights resulting from different starting average lignin molecular weights were determined for comparison with experimental results from Marathe et al.⁴⁴ This comparison is shown in Figure 9. For the model, the labile bond propensity was kept at 0.45, recombination propensity was 0.84 (for 530 °C reported experimental temperature), and aerosol propensities of 0.15 and 0.05 were used for low and high pressures,

respectively. Evaporation of model tetramers was allowed for low pressure but not for high pressure. Monomers, dimers, and trimers evaporate at both low and high pressures.

These results show that the proposed model reproduces the experimental trends shown by Marathe et al. 44 For "light" lignin (Da < ~400), parity is preserved between the lignin molecular weight and resulting oil. This is the result of the direct evaporation of the "light" lignin with a very limited extent of pyrolysis reactions. 44 For "heavier" lignin, the oil molecular weight is bifurcated based on pressure. At lower pressure, heavier lignin oligomers can evaporate during pyrolysis, thereby yielding an overall heavier oil. At higher pressure, these heavier oligomers do not evaporate, thereby vielding an overall lighter oil. Model results show a slowly increasing oil molecular weight with respect to the starting lignin molecular weight. Marathe et al. suggest a more constant oil molecular weight, although their lignins differ in the labile β -O-4 content, with appreciable experimental uncertainty among the results. 44 A higher labile bond propensity naturally corresponds to lighter resulting oils and a higher overall oil yield. Similarly, a lower recombination propensity (i.e., higher temperature) corresponds to more oil and less char. The proposed integrated model is capable of reproducing these trends. The relationship between the model parameter space and the resulting oil and char yields is shown in the Supporting Information.

3.6. Discussion. The characterization of hybrid poplar MWL revealed that FT-ICR MS-detected lignin molecules were made up of oligomeric units with 3, 4, and 5 aromatic rings (Figure 3). This set of MWL oligomers was well described by a library of hypothetical/computational structures developed through the stochastic generation of modified short linear oligomers. The FT-ICR MS-detected products from the pyrolysis of MWL were similarly made up of lignin-derived trimers and tetramers, with a much smaller amount of dimers and pentamers (Figure 4, Figure S2). Comparative analysis between abundant products and raw MWL suggests that during pyrolysis, there is a significant shift toward the lower molecular weight and decreased O/C ratio (Figures 4 and 7).

The various interunit bonds connecting lignin monomers have a range of bond dissociation enthalpies. Ether linkages, such as β -O-4, tend to be \sim 60–70 kcal/mol, while C–C bonds tend to be \sim 100 kcal/mol. ^{80–84} The location of a given bond in a lignin oligomeric unit can also have an impact on its dissociation enthalpy for β -O-4 homolytic cleavage. ⁸⁵ Because



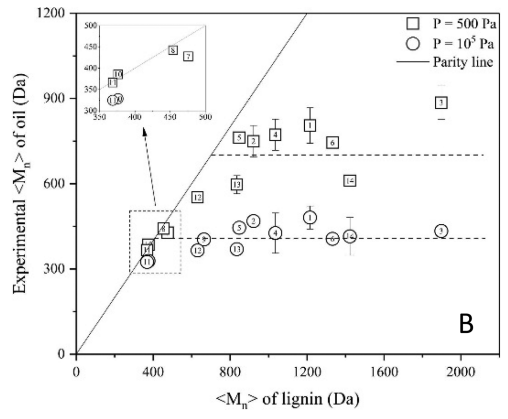


Figure 9. Comparison between molecular weight of lignin pyrolysis oil for (A) model results and (B) experimental results (reproduced from Marathe et al.⁴⁴

of bond dissociation enthalpy disparities between C-O and C-C bonds, during the early stages of pyrolysis, there should be preferential cleavage of ether linkages. 86,87 During these primary reactions (e.g., ether cleavage, demethoxylation, decarboxylation, and deacylation)⁴⁵ that result in deoxygenation and molecular weight decreases for initial MWL, oligomers with a sufficiently low vaporization temperature are formed and subsequently devolatilized directly from the reaction front. Boiling point correlation analysis (Figure 8) suggests that these oligomers should be primarily made up of lignin trimers. The presence of heavier molecules may be the result of reactive boiling/aerosol ejections, although this contribution to the total oligomer pool is less significant than direct vaporization. The presence of directly vaporized oligomers does not preclude the recombination of monomers into heavier species during the complicated interplay of chemical and physical processes in early pyrolysis reactions. For example, Li et al., report that "simple" pyrolytic lignin monomers, dimers, and coke could be formed from the recombination of monomeric model compounds; however, "complex" oligomeric pyrolytic lignin could only be derived from the fragmentation of whole/real lignin. 86 This supports the hypothesis that oligomer products are detectable in lignin pyrolysis oil largely due to their direct vaporization during the early stages of pyrolysis. An ongoing challenge for understanding the nature of oligomer formation is the reliable collection of these products during pyrolysis and accurately analyzing them with suitable techniques. Wentrup has recently published a thorough review of the analytical capabilities of flash vacuum pyrolysis in general (not strictly for biomass), which may provide useful insights for the development of innovative reactor designs for biomass.8

Several other successful modeling approaches of lignin pyrolysis appropriately incorporate transport phenomena such as vaporization. 44-46,59 One illustrative example is the flash distillation analogy employed by Niksa in the bio-FLASH-CHAIN model.⁴⁶ In this model, tar precursors are in phase equilibrium with liquid tar products following Henry's law relationship.⁸⁹ Chemical reaction modeling alone—of model compounds especially but also for whole lignin—falls short in capturing the true nature of lignin decomposition in pyrolysis. Primary processes yield a high volume of a wide variety of product species as the result of nonchemical devolatilization (such as vaporization and aerosol ejection). These devolatilization mechanisms must be explicitly accounted for to accurately model a given liquefaction process. The flash distillation analogy for devolatilization is also employed for coal pyrolysis in the CPD model, described by Fletcher. 90 Similar interpretations of evaporation-driven "heavy" product collection have also been reported for the pyrolysis of used tire particles, cellulose, and polyethylene. 91–93

The advantage of our proposed approach, using a stochastic modeling strategy of the MWL structure⁵⁶ (in contrast to pseudocomponent models)^{59,94} and combinatorics-based functional group expansion (Figure 5), is in molecular-level speciation from the beginning. With proper structural/conformational analysis, thermophysical/chemical properties (e.g., vaporization curves, solubility parameters) for both reactants and products and pyrolysis/liquefaction product yields may be more accurately determined. This leaves a plethora of directions for future studies, including advancing applications of density functional theory for rigorous structure determination and analytical chemistry (e.g., FTIR and NMR)

data prediction with experimental validation. From a practical perspective, incorporating the effect of pressure into the understanding of lignin pyrolysis can potentially allow for new levels of control over product characteristics. By operating at lower pressures, higher oligomer and total oil yields have been observed, with lower char yields. However, monomer yields are largely independent of the reactor pressure. Operating at higher external pressures has been shown to improve char yields and solid carbon retention, which has practical implications on carbonization technologies aimed at the biochar or charcoal production from whole biomass. ^{95,96}

4. CONCLUSIONS

The characterization and stochastic modeling of milled wood lignin structures shows that it is well described as a combination of linear oligomers with three to five aromatic rings with the known overall chemical formulas. Further analysis of pyrolysis products suggests that structures can be proposed for these products based on the simple modifications of the starting milled wood lignin constitutive oligomers. This is based on the observation that primary pyrolysis products are oligomers with an apparent high degree of formula and structural similarity to the initial milled wood lignin. Further, based on the analysis of thermophysical/chemical (e.g., boiling point, heat of vaporization) properties and integrated probabilistic/stochastic modeling, there is evidence to suggest that the predominant mode of pyrolytic lignin formation and/ or collection is from direct vaporization with a limited extent of reactions. Based on these results, opportunities for future work are highlighted. These include rigorous computational analyses (e.g., density functional theory) and experimental validation of initial lignin oligomer structures, pyrolysis pathways, and oligomer product structures. Attempting modeling work with initial molecular-level detail does, however, come at the expense of a potentially much higher computational cost. Improvements in the accuracy of correlations to estimate physical and/or chemical properties from molecular structures, particularly with regard to biomass-derived oligomers, may also be of great benefit. An important factor that must be considered when studying lignin pyrolysis is the inclusion of the effect of pressure on mass transport phenomena. Pressure plays an important, nonkinetic role in the yield and characteristics of pyrolysis products from lignin. In particular, lower (subatmospheric) pressures induce more oligomer vaporization, resulting in less char and heavier pyrolysis oil; monomer yields are essentially pressure-independent. Ultimately, the goal of this study and the proposed trajectory of future work are centered on the development of improved microkinetic models aimed at more successful lignin valorization.

ASSOCIATED CONTENT

Supporting Information

The Supporting Information is available free of charge at https://pubs.acs.org/doi/10.1021/acs.energy fuels.0c02928.

Description of algorithm and details of the lignin model; van Krevelen diagram and H/C ratio vs mass plots for pyrolysis products with FT-ICR MS intensity; complete results of statistical analysis comparing lignin and pyrolysis products; details of boiling point correlation calculations; relationship between the model parameter space and the resulting oil and char yields; milled wood

lignin extraction; and details of physical characteristics (PDF)

AUTHOR INFORMATION

Corresponding Author

Manuel Garcia-Perez — Biological Systems Engineering and Bioproducts, Sciences & Engineering Laboratory, Washington State University, Pullman, Washington 99163, United States; orcid.org/0000-0002-9386-2632; Phone: 509-372-7461; Email: mgarcia-perez@wsu.edu

Author

Evan Terrell — Biological Systems Engineering, Washington State University, Pullman, Washington 99163, United States; orcid.org/0000-0002-1079-4110

Complete contact information is available at: https://pubs.acs.org/10.1021/acs.energyfuels.0c02928

Notes

The authors declare no competing financial interest.

■ ACKNOWLEDGMENTS

The authors acknowledge the financial contributions received from the U.S. Department of Energy (DE-EE0008505) and the U.S. National Science Foundation (NSF-CBET 1926412). Dr. Garcia-Perez is also very thankful to the U.S. Department of Agriculture's National Institute of Food and Agriculture through the Hatch Project (WNP00701) for funding his research program. Lina Martinez is also gratefully acknowledged for fruitful discussions on pyrolysis modeling.

■ REFERENCES

- (1) Li, C.; Zhao, X.; Wang, A.; Huber, G. W.; Zhang, T. Catalytic Transformation of Lignin for the Production of Chemicals and Fuels. *Chem. Rev.* **2015**, *115*, 11559–11624.
- (2) Luo, H.; Abu-Omar, M. M. Lignin Extraction and Catalytic Upgrading from Genetically Modified Poplar. *Green Chem.* **2018**, 20, 745–753
- (3) Sanderson, K. Lignocellulose: A Chewy Problem. *Nature* 2011, 474, S12-S14.
- (4) Shuai, L.; Talebi Amiri, M.; Luterbacher, J. S. The Influence of Interunit Carbon—Carbon Linkages during Lignin Upgrading. *Curr. Opin. Green Sustain. Chem.* **2016**, *2*, 59–63.
- (5) Chen, D.; Gao, A.; Cen, K.; Zhang, J.; Cao, X.; Ma, Z. Investigation of Biomass Torrefaction Based on Three Major Components: Hemicellulose, Cellulose, and Lignin. *Energy Convers. Manage.* **2018**, *169*, 228–237.
- (6) Schutyser, W.; Renders, T.; Van Den Bosch, S.; Koelewijn, S. F.; Beckham, G. T.; Sels, B. F. Chemicals from Lignin: An Interplay of Lignocellulose Fractionation, Depolymerisation, and Upgrading. *Chem. Soc. Rev.* **2018**, *47*, 852–908.
- (7) Sun, Z.; Fridrich, B.; De Santi, A.; Elangovan, S.; Barta, K. Bright Side of Lignin Depolymerization: Toward New Platform Chemicals. *Chem. Rev.* **2018**, *118*, 614–678.
- (8) Zhang, C.; Wang, F. Catalytic Lignin Depolymerization to Aromatic Chemicals. Acc. Chem. Res. 2020, 53, 470.
- (9) Garedew, M.; Lin, F.; Song, B.; DeWinter, T. M.; Jackson, J. E.; Saffron, C. M.; Lam, C. H.; Anastas, P. Greener Routes to Biomass Waste Valorization: Lignin Transformation Through Electrocatalysis for Renewable Chemicals and Fuels Production. *ChemSusChem* **2020**, *13*, cssc.202000987.
- (10) Ponnusamy, V. K.; Nguyen, D. D.; Dharmaraja, J.; Shobana, S.; Banu, J. R.; Saratale, R. G.; Chang, S. W.; Kumar, G. A Review on Lignin Structure, Pretreatments, Fermentation Reactions and Biorefinery Potential. *Bioresour. Technol.* **2019**, 271, 462–472.

- (11) Albishi, T.; Mikhael, A.; Shahidi, F.; Fridgen, T. D.; Delmas, M.; Banoub, J. Top-down Lignomic Matrix-Assisted Laser Desorption/Ionization Time-of-Flight Tandem Mass Spectrometry Analysis of Lignin Oligomers Extracted from Date Palm Wood. *Rapid Commun. Mass Spectrom.* **2019**, 33, 539–560.
- (12) Banoub, J.; Delmas, G. H.; Joly, N.; Mackenzie, G.; Cachet, N.; Benjelloun-Mlayah, B.; Delmas, M. A Critique on the Structural Analysis of Lignins and Application of Novel Tandem Mass Spectrometric Strategies to Determine Lignin Sequencing. *J. Mass Spectrom.* **2015**, *50*, 5–48.
- (13) Mikhael, A.; Jurcic, K.; Fridgen, T. D.; Delmas, M.; Banoub, J. Matrix-Assisted Laser Desorption/Ionization Time-of-Flight/Time-of-Flight Tandem Mass Mass Spectrometry (Negative Ion Mode) of French Oak Lignin: A Novel Series of Lignin and Tricin Derivatives Attached to Carbohydrate and Shikimic Acid Moieties. *Rapid Commun. Mass Spectrom.* **2020**, *34*, 8841.
- (14) Crestini, C.; Melone, F.; Sette, M.; Saladino, R. Milled Wood Lignin: A Linear Oligomer. *Biomacromolecules* **2011**, *12*, 3928–3935.
- (15) Chang, H. M.; Jiang, X. Biphenyl Structure and Its Impact on the Macromolecular Structure of Lignin: A Critical Review. *J. Wood Chem. Technol.* **2020**, *40*, 81–90.
- (16) Ralph, J.; Lundquist, K.; Brunow, G.; Lu, F.; Kim, H.; Schatz, P. F.; Marita, J. M.; Hatfield, R. D.; Ralph, S. A.; Christensen, J. H.; et al. Lignins: Natural Polymers from Oxidative Coupling of 4-Hydroxyphenyl- Propanoids. *Phytochem. Rev.* **2004**, *3*, 29–60.
- (17) Ralph, J.; Lapierre, C.; Boerjan, W. Lignin Structure and Its Engineering. *Curr. Opin. Biotechnol.* **2019**, *56*, 240–249.
- (18) Rencoret, J.; Neiva, D.; Marques, G.; Gutiérrez, A.; Kim, H.; Gominho, J.; Pereira, H.; Ralph, J.; del Río, J. C. Hydroxystilbene Glucosides Are Incorporated into Norway Spruce Bark Lignin. *Plant Physiol.* **2019**, *180*, 1310–1321.
- (19) Del Río, J. C.; Rencoret, J.; Gutiérrez, A.; Elder, T.; Kim, H.; Ralph, J. Lignin Monomers from beyond the Canonical Monolignol Biosynthetic Pathway: Another Brick in the Wall. *ACS Sustainable Chem. Eng.* **2020**, *8*, 4997–5012.
- (20) Lupoi, J. S.; Singh, S.; Parthasarathi, R.; Simmons, B. A.; Henry, R. J. Recent Innovations in Analytical Methods for the Qualitative and Quantitative Assessment of Lignin. *Renew. Sustain. Energy Rev.* **2015**, 49, 871–906.
- (21) Qi, Y.; Fu, P.; Li, S.; Ma, C.; Liu, C.; Volmer, D. A. Assessment of Molecular Diversity of Lignin Products by Various Ionization Techniques and High-Resolution Mass Spectrometry. *Sci. Total Environ.* **2020**, 713, 136573.
- (22) Kubátová, A.; Andrianova, A. A.; Hatton, J.; Kozliak, E. I. Atmospheric Pressure Ionization Mass Spectrometry as a Tool for Structural Characterization of Lignin. *Rapid Commun. Mass Spectrom.* **2020**, *34*, e8813.
- (23) Prothmann, J.; Li, K.; Hulteberg, C.; Spégel, P.; Sandahl, M.; Turner, C. Non-Targeted Analysis Strategy for the Identification of Phenolic Compounds in Complex Technical Lignin Samples. *ChemSusChem* **2020**, *13*, 4605–4612.
- (24) Bowman, A. S.; Asare, S. O.; Lynn, B. C. Matrix-Assisted Laser Desorption/Ionization Time-of-Flight Mass Spectrometry Analysis for Characterization of Lignin Oligomers Using Cationization Techniques and 2,5-Dihydroxyacetophenone (DHAP) Matrix. *Rapid Commun. Mass Spectrom.* **2019**, 33, 811–819.
- (25) Marshall, A. G. Milestones in Fourier Transform Ion Cyclotron Resonance Mass Spectrometry Technique Development. *Int. J. Mass Spectrom.* **2000**, 200, 331–356.
- (26) Cho, Y.; Ahmed, A.; Islam, A.; Kim, S. Developments in FT-ICR MS Instrumentation, Ionization Techniques, and Data Interpretation Methods for Petroleomics. *Mass Spectrom. Rev.* **2015**, 34, 248–263.
- (27) Nikolaev, E. N.; Kostyukevich, Y. I.; Vladimirov, G. N. Fourier Transform Ion Cyclotron Resonance (FT ICR) Mass Spectrometry: Theory and Simulations. *Mass Spectrom. Rev.* **2016**, *35*, 219–258.
- (28) Hertzog, J.; Carré, V.; Le Brech, Y.; Mackay, C. L.; Dufour, A.; Mašek, O.; Aubriet, F. Combination of Electrospray Ionization, Atmospheric Pressure Photoionization and Laser Desorption

- Ionization Fourier Transform Ion Cyclotronic Resonance Mass Spectrometry for the Investigation of Complex Mixtures Application to the Petroleomic Analysis. *Anal. Chim. Acta* **2017**, *969*, 26–34.
- (29) Shrestha, B.; Le Brech, Y.; Ghislain, T.; Leclerc, S.; Carré, V.; Aubriet, F.; Hoppe, S.; Marchal, P.; Pontvianne, S.; Brosse, N.; et al. A Multitechnique Characterization of Lignin Softening and Pyrolysis. ACS Sustainable Chem. Eng. 2017, 5, 6940–6949.
- (30) Terrell, E.; Carré, V.; Dufour, A.; Aubriet, F.; le Brech, Y.; Garcia-Pérez, M. Contributions to Lignomics: Stochastic Generation of Oligomeric Lignin Structures for Interpretation of MALDI-FT-ICR-MS Results. *ChemSusChem* **2020**, *13*, 4428–4445.
- (31) Aubriet, F.; Ghislain, T.; Hertzog, J.; Sonnette, A.; Dufour, A.; Mauviel, G.; Carré, V. Characterization of Biomass and Biochar by LDI-FTICRMS Effect of the Laser Wavelength and Biomass Material. J. Am. Soc. Mass Spectrom. 2018, 29, 1951–1962.
- (32) McClelland, D. J.; Motagamwala, A. H.; Li, Y.; Rover, M. R.; Wittrig, A. M.; Wu, C.; Buchanan, J. S.; Brown, R. C.; Ralph, J.; Dumesic, J. A.; et al. Functionality and Molecular Weight Distribution of Red Oak Lignin before and after Pyrolysis and Hydrogenation. *Green Chem.* **2017**, *19*, 1378–1389.
- (33) Ware, R. L.; Rodgers, R. P.; Marshall, A. G.; Mante, O. D.; Dayton, D. C.; Verdier, S.; Gabrielsen, J.; Rowland, S. M. Detailed Chemical Composition of an Oak Biocrude and Its Hydrotreated Product Determined by Positive Atmospheric Pressure Photoionization Fourier Transform Ion Cyclotron Resonance Mass Spectrometry. Sustain. Energy Fuels 2020, 4, 2404–2410.
- (34) Zherebker, A.; Rukhovich, G. D.; Kharybin, O.; Fedoros, E. I.; Perminova, I. V.; Nikolaev, E. N. FTICR-MS for the Analysis of Molecular Composition Ad Batch-to-Batch Consistency of Plant Derived Polyphenolic Ligand Developed for Biomedical Application. *Rapid Commun. Mass Spectrom.* 2020, 34, e8850.
- (35) Echavarri-Bravo, V.; Tinzl, M.; Kew, W.; Cruickshank, F.; Logan Mackay, C.; Clarke, D. J.; Horsfall, L. E. High Resolution Fourier Transform Ion Cyclotron Resonance Mass Spectrometry (FT-ICR MS) for the Characterisation of Enzymatic Processing of Commercial Lignin. New Biotechnol. 2019, 52, 1–8.
- (36) Olcese, R.; Carré, V.; Aubriet, F.; Dufour, A. Selectivity of Bio-Oils Catalytic Hydrotreatment Assessed by Petroleomic and GC*GC/MS-FID Analysis. *Energy Amp. Fuels* **2013**, *27*, 2135–2145.
- (37) Collard, F. X.; Blin, J. A Review on Pyrolysis of Biomass Constituents: Mechanisms and Composition of the Products Obtained from the Conversion of Cellulose, Hemicelluloses and Lignin. *Renew. Sustain. Energy Rev.* **2014**, *38*, 594–608.
- (38) Garcia-Perez, M.; Wang, S.; Shen, J.; Rhodes, M.; Lee, W. J.; Li, C. Z. Effects of Temperature on the Formation of Lignin-Derived Oligomers during the Fast Pyrolysis of Mallee Woody Biomass. *Energy Fuels* **2008**, *22*, 2022–2032.
- (39) Garcia-Perez, M.; Wang, X. S.; Shen, J.; Rhodes, M. J.; Tian, F.; Lee, W. J.; Wu, H.; Li, C. Z. Fast Pyrolysis of Oil Mallee Woody Biomass: Effect of Temperature on the Yield and Quality of Pyrolysis Products. *Ind. Eng. Chem. Res.* **2008**, *47*, 1846–1854.
- (40) Bai, X.; Kim, K. H.; Brown, R. C.; Dalluge, E.; Hutchinson, C.; Lee, Y. J.; Dalluge, D. Formation of Phenolic Oligomers during Fast Pyrolysis of Lignin. *Fuel* **2014**, *128*, 170–179.
- (41) Patwardhan, P. R.; Brown, R. C.; Shanks, B. H. Understanding the Fast Pyrolysis of Lignin. *ChemSusChem* **2011**, *4*, 1629–1636.
- (42) Zhou, S.; Pecha, B.; van Kuppevelt, M.; McDonald, A. G.; Garcia-Perez, M. Slow and Fast Pyrolysis of Douglas-Fir Lignin: Importance of Liquid-Intermediate Formation on the Distribution of Products. *Biomass Bioenergy* **2014**, *66*, 398–409.
- (43) Zhou, S.; Garcia-Perez, M.; Pecha, B.; McDonald, A. G.; Kersten, S. R. A.; Westerhof, R. J. M. Secondary Vapor Phase Reactions of Lignin-Derived Oligomers Obtained by Fast Pyrolysis of Pine Wood. *Energy Fuels* **2013**, *27*, 1428–1438.
- (44) Marathe, P. S.; Westerhof, R. J. M.; Kersten, S. R. A. Fast Pyrolysis of Lignins with Different Molecular Weight: Experiments and Modelling. *Appl. Energy* **2019**, 236, 1125–1137.

- (45) Yanez, A. J.; Natarajan, P.; Li, W.; Mabon, R.; Broadbelt, L. J. Coupled Structural and Kinetic Model of Lignin Fast Pyrolysis. *Energy Fuels* **2018**, *32*, 1822–1830.
- (46) Niksa, S. Bio -FLASHCHAIN ® Theory for Rapid Devolatilization of Biomass 1. Lignin Devolatilization. *Fuel* **2019**, 263, 116649.
- (47) Terrell, E.; Dellon, L. D.; Dufour, A.; Bartolomei, E.; Broadbelt, L. J.; Garcia-Perez, M. A Review on Lignin Liquefaction: Advanced Characterization of Structure and Microkinetic Modeling. *Ind. Eng. Chem. Res.* **2020**, *59*, 526–555.
- (48) Pecha, M. B.; Arbelaez, J. I. M.; Garcia-Perez, M.; Chejne, F.; Ciesielski, P. N. Progress in Understanding the Four Dominant Intra-Particle Phenomena of Lignocellulose Pyrolysis: Chemical Reactions, Heat Transfer, Mass Transfer, and Phase Change. *Green Chem.* **2019**, 21, 2868–2898.
- (49) Marathe, P. S.; Westerhof, R. J. M.; Kersten, S. R. A. Effect of Pressure and Hot Vapor Residence Time on the Fast Pyrolysis of Biomass: Experiments and Modeling. *Energy Fuels* **2020**, *34*, 1773–1780
- (50) Terrell, E.; Garcia-Perez, M. Novel Strategy To Analyze Fourier Transform Ion Cyclotron Resonance Mass Spectrometry Data of Biomass Pyrolysis Oil for Oligomeric Structure Assignment. *Energy Fuels* **2020**, 34, 8466–8481.
- (51) Pecha, M. B.; Terrell, E.; Montoya, J. I.; Stankovikj, F.; Broadbelt, L. J.; Chejne, F.; Garcia-Perez, M. Effect of Pressure on Pyrolysis of Milled Wood Lignin and Acid-Washed Hybrid Poplar Wood. *Ind. Eng. Chem. Res.* **2017**, *56*, 9079–9089.
- (52) Zhou, S.; Wang, Z.; Liaw, S. S.; Li, C. Z.; Garcia-Perez, M. Effect of Sulfuric Acid on the Pyrolysis of Douglas Fir and Hybrid Poplar Wood: Py-GC/MS and TG Studies. *J. Anal. Appl. Pyrolysis* **2013**, *104*, 117–130.
- (53) Björkman, A. Isolation of Lignin from Finely Divided Wood with Neutral Solvents. *Nature* **1954**, *174*, 1057–1058.
- (54) Björkman, A. Lignin and Lignin-Carbohydrate Complexes Extraction from Wood Meal with Neutral Solvents. *Ind. Eng. Chem.* **1957**, *49*, 1395–1398.
- (55) Obst, J. R.; Kirk, T. K. Isolation of Lignin. *Methods Enzymol.* **1985**, *161*, 3–12.
- (56) Dellon, L. D.; Yanez, A. J.; Li, W.; Mabon, R.; Broadbelt, L. J. Computational Generation of Lignin Libraries from Diverse Biomass Sources. *Energy Fuels* **2017**, *31*, 8263–8274.
- (57) Pecha, M. B.; Montoya, J. I.; Ivory, C.; Chejne, F.; Garcia-Perez, M. Modified Pyroprobe Captive Sample Reactor: Characterization of Reactor and Cellulose Pyrolysis at Vacuum and Atmospheric Pressures. *Ind. Eng. Chem. Res.* **2017**, *56*, 5185–5200.
- (58) Monteiro, M. J. Fitting Molecular Weight Distributions Using a Log-Normal Distribution Model. *Eur. Polym. J.* **2015**, *65*, 197–201.
- (59) Faravelli, T.; Frassoldati, A.; Migliavacca, G.; Ranzi, E. Detailed Kinetic Modeling of the Thermal Degradation of Lignins. *Biomass Bioenergy* **2010**, *34*, 290–301.
- (60) Montoya, J.; Pecha, B.; Janna, F. C.; Garcia-Perez, M. Single Particle Model for Biomass Pyrolysis with Bubble Formation Dynamics inside the Liquid Intermediate and Its Contribution to Aerosol Formation by Thermal Ejection. *J. Anal. Appl. Pyrolysis* **2017**, 124, 204–218.
- (61) Kim, S.; Kramer, R. W.; Hatcher, P. G. Graphical Method for Analysis of Ultrahigh-Resolution Broadband Mass Spectra of Natural Organic Matter, the Van Krevelen Diagram. *Anal. Chem.* **2003**, *75*, 5336–5344.
- (62) Hertzog, J.; Carré, V.; Le Brech, Y.; Dufour, A.; Aubriet, F. Toward Controlled Ionization Conditions for ESI-FT-ICR-MS Analysis of Bio-Oils from Lignocellulosic Material. *Energy Fuels* **2016**, *30*, 5729–5739.
- (63) Hockaday, W. C.; Grannas, A. M.; Kim, S.; Hatcher, P. G. Direct Molecular Evidence for the Degradation and Mobility of Black Carbon in Soils from Ultrahigh-Resolution Mass Spectral Analysis of Dissolved Organic Matter from a Fire-Impacted Forest Soil. *Org. Geochem.* **2006**, *37*, 501–510.

- (64) Altgelt, K. H.; Boduszynski, M. M. Composition of Heavy Petroleums. 3. An Improved Boiling Point-Molecular Weight Relation. *Energy Fuels* **1992**, *6*, 68–72.
- (65) Twu, C. H. An Internally Consistent Correlation for Predicting the Critical Properties and Molecular Weights of Petroleum and Coal-Tar Liquids. *Fluid Phase Equilib.* **1984**, *16*, 137–150.
- (66) Satou, M.; Itoh, D.; Hattori, H.; Yoshida, T. Evaluation of Ring Size Distribution in a Heavy Oil Based on Boiling Point and Molecular Weight Distributions. *Fuel* **2000**, *79*, 339–348.
- (67) Jianzhong, Z.; Suoqi, Z.; Renan, W.; Guanghua, Y. Prediction of Critical Properties of Non-Polar Compounds, Petroleum and Coal-Tar Liquids. *Fluid Phase Equilib.* **1998**, *149*, 103–109.
- (68) Yuan, W.; Hansen, A.; Zhang, Q. Vapor Pressure and Normal Boiling Point Predictions for Pure Methyl Esters and Biodiesel Fuels. *Fuel* **2005**, *84*, 943–950.
- (69) Teja, A. S.; Lee, R. J.; Rosenthal, D.; Anselme, M. Correlation of the Critical Properties of Alkanes and Alkanols. *Fluid Phase Equilib.* **1990**, *56*, 153–169.
- (70) Dearden, J. C. Quantitative Structure-Property Relationships for Prediction of Boiling Point, Vapor Pressure, and Melting Point. *Environ. Toxicol. Chem.* **2003**, 22, 1696–1709.
- (71) Katritzky, A. R.; Kuanar, M.; Slavov, S.; Hall, C. D.; Karelson, M.; Kahn, I.; Dobchev, D. A. Quantitative Correlation of Physical and Chemical Properties with Chemical Structure: Utility for Prediction. *Chem. Rev.* **2010**, *110*, 5714–5789.
- (72) Gani, R. Group Contribution-Based Property Estimation Methods: Advances and Perspectives. *Curr. Opin. Chem. Eng.* **2019**, 23, 184–196.
- (73) Montoya, J.; Pecha, B.; Janna, F. C.; Garcia-Perez, M. Methodology for Estimation of Thermal Ejection Droplet Size Distribution and Intensity during the Pyrolysis of Sugarcane Bagasse and Model Compounds. *J. Anal. Appl. Pyrolysis* **2017**, *125*, 69–82.
- (74) Tiarks, J. A.; Dedic, C. E.; Meyer, T. R.; Brown, R. C.; Michael, J. B. Visualization of Physicochemical Phenomena during Biomass Pyrolysis in an Optically Accessible Reactor. *J. Anal. Appl. Pyrolysis* **2019**, *143*, 104667.
- (75) Zhao, L.; Ni, N.; Yalkowsky, S. H. A Modification of Trouton's Rule by Simple Molecular Parameters for Hydrocarbon Compounds. *Ind. Eng. Chem. Res.* **1999**, 38, 324–327.
- (76) Montoya, J.; Pecha, B.; Janna, F. C.; Garcia-Perez, M. Micro-Explosion of Liquid Intermediates during the Fast Pyrolysis of Sucrose and Organosolv Lignin. *J. Anal. Appl. Pyrolysis* **2016**, 122, 106–121.
- (77) Capanema, E. A.; Balakshin, M. Y.; Kadla, J. F. Quantitative Characterization of a Hardwood Milled Wood Lignin by Nuclear Magnetic Resonance Spectroscopy. *J. Agric. Food Chem.* **2005**, *53*, 9639–9649.
- (78) Garcia-Perez, M.; Chaala, A.; Pakdel, H.; Kretschmer, D.; Roy, C. Characterization of Bio-Oils in Chemical Families. *Biomass Bioenergy* **2007**, *31*, 222–242.
- (79) Bartolomei, E.; Le Brech, Y.; Dufour, A.; Carre, V.; Aubriet, F.; Terrell, E.; Garcia-Perez, M.; Arnoux, P. Lignin Depolymerization: A Comparison of Methods to Analyze Monomers and Oligomers. *ChemSusChem* **2020**, *13*, 1–4648.
- (80) Kim, S.; Chmely, S. C.; Nimlos, M. R.; Bomble, Y. J.; Foust, T. D.; Paton, R. S.; Beckham, G. T. Computational Study of Bond Dissociation Enthalpies for a Large Range of Native and Modified Lignins. *J. Phys. Chem. Lett.* **2011**, *2*, 2846–2852.
- (81) Parthasarathi, R.; Romero, R. A.; Redondo, A.; Gnanakaran, S. Theoretical Study of the Remarkably Diverse Linkages in Lignin. *J. Phys. Chem. Lett.* **2011**, *2*, 2660–2666.
- (82) Beste, A.; Buchanan, A. C. Computational Study of Bond Dissociation Enthalpies for Lignin Model Compounds. Substituent Effects in Phenethyl Phenyl Ethers. *J. Org. Chem.* **2009**, *74*, 2837–2841.
- (83) Elder, T. Bond Dissociation Enthalpies of a Pinoresinol Lignin Model Compound. *Energy Fuels* **2014**, 28, 1175–1182.
- (84) Elder, T. Bond Dissociation Enthalpies of a Dibenzodioxocin Lignin Model Compound. *Energy Fuels* **2013**, *27*, 4785–4790.

- (85) Azad, T.; Schuler, J.; Auad, M.; Elder, T.; Adamczyk, A. Model Lignin Oligomer Pyrolysis: Coupled Conformational and Thermodynamic Analysis of β -O-4' Bond Cleavage. *Energy Fuels* **2020**, *34*, 9709–9724
- (86) Li, S.; Luo, Z.; Wang, W.; Lu, K.; Yang, Y.; Liang, X. Characterization of Pyrolytic Lignin and Insight into Its Formation Mechanisms Using Novel Techniques and DFT Method. *Fuel* **2020**, 262, 116516.
- (87) Kotake, T.; Kawamoto, H.; Saka, S. Mechanisms for the Formation of Monomers and Oligomers during the Pyrolysis of a Softwood Lignin. *J. Anal. Appl. Pyrolysis* **2014**, *105*, 309–316.
- (88) Wentrup, C. Flash Vacuum Pyrolysis: Techniques and Reactions. *Angew. Chem. Int. Ed.* **2017**, *56*, 14808–14835.
- (89) Niksa, S. Rapid Coal Devolatilization as an Equilibrium Flash Distillation. *AIChE J.* **1988**, *34*, 790–802.
- (90) Fletcher, T. H. Review of 30 Years of Research Using the Chemical Percolation Devolatilization Model. *Energy Fuels* **2019**, 33, 12123–12153.
- (91) Yang, J.; Tanguy, P. A.; Roy, C. Heat Transfer, Mass Transfer and Kinetics Study of the Vacuum Pyrolysis of a Large Used Tire Particle. *Chem. Eng. Sci.* **1995**, *50*, 1909–1922.
- (92) Suuberg, E. M.; Milosavljevic, I.; Oja, V. Two-Regime Global Kinetics of Cellulose Pyrolysis: The Role of Tar Evaporation. *Symp. Combust.* **1996**, *26*, 1515–1521.
- (93) Sezgi, N. A.; Cha, W. S.; Smith, J. M.; McCoy, B. J. Polyethylene Pyrolysis: Theory and Experiments for Molecular-Weight-Distribution Kinetics. *Ind. Eng. Chem. Res.* **1998**, 37, 2582–2591.
- (94) Hough, B. R.; Schwartz, D. T.; Pfaendtner, J. Detailed Kinetic Modeling of Lignin Pyrolysis for Process Optimization. *Ind. Eng. Chem. Res.* **2016**, *55*, 9147–9153.
- (95) Wang, L.; Trninic, M.; Skreiberg, O.; Gronli, M.; Considine, R.; Antal, M. J. Is Elevated Pressure Required to Achieve a High Fixed-Carbon Yield of Charcoal from Biomass? Part 1: Round-Robin Results for Three Different Corncob Materials. *Energy Fuels* **2011**, 25, 3251–3265.
- (96) Wang, L.; Skreiberg, Ø.; Gronli, M.; Specht, G. P.; Antal, M. J. Is Elevated Pressure Required to Achieve a High Fixed-Carbon Yield of Charcoal from Biomass? Part 2: The Importance of Particle Size. *Energy Fuels* **2013**, *27*, 2146–2156.